Application of a kinetic model to tracer diffusion of silicon and oxygen in silicate melts

1994 J. Phys.: Condens. Matter 6 9835

(http://iopscience.iop.org/0953-8984/6/46/004)

J. Phys.: Condens. Matter 6 (1994) 9835–9852. Printed in the UK

Application of a kinetic model to tracer diffusion of silicon and oxygen in silicate melts

T F Young†‡, J Kieffer†§ and G Borchardt†

† Institut für Allgemeine Metallurgie, Technische Universität Clausthal, D-38678 Clausthal-Zellerfeld, Germany

‡ Department of Physics, National Sun Yat-Sen University, Kaohsiung, Taiwan, Republic of China 80424

§ Department of Materials Science and Engineering, University of Illinois, Urbana, IL 61801, USA

Received 17 March 1994, in final form 18 July 1994

Abstract. In this work we have improved the kinetic model of Kieffer and Borchardt for diffusion in silicate melts, which takes into account both the diffusion of individual polyanions and the reaction of different polyanions through condensation and splitting events. Making assumptions for the individual condensation reactions, similar to those by Masson, the equilibrium polyanion distributions in silicate melts were calculated by solving a system of coupled first-order differential equations, describing the reactions between polyanions of various sizes. The concentration dependence of the SiO_4^{4-} monomers, determined by our approach, is identical to that resulting from the thermodynamic treatment by Masson. Furthermore, by allowing for local changes in the isotope distributions of the elements, and by assuming that migration of all species present in the system occurs due to random motion, the self-diffusion of silicon and oxygen in $CoO–SiO_2$ melts has been simulated. The parameters for the model have been estimated by fitting the simulation results to our experimental data of Si and O tracer diffusion. While the simulated concentration profiles were in good agreement with our experimental tracer diffusion measurements in the $CoO–SiO_2$ system, their shape could not be described by the standard solution of Fick's law. Conversely, for the $CaO–SiO_2$ and $PbO–SiO_2$ systems, the simulated profiles were in much better agreement with the standard solution. This difference in diffusional transport properties can be qualitatively interpreted as due to the structural differences of $CoO–SiO_2$ as compared to the two other systems.

1. Introduction

The properties of silicate melts, e.g. the viscosity and the electrical and thermal conductivity, depend very sensitively on the chemical composition and on the nature of the constituents. An increase in temperature not only enhances atomic mobility by providing the necessary activation energy, it also alters the degree of networking in the equilibrium structure. To date, a number of models have been proposed by several authors [1–6] for the description of the structure of silicate melts. These models are mostly based on thermodynamic formalisms. While the relationships between structure and thermodynamic properties have been explored extensively, attempts to relate the mobilities of structural constituents to the geometry of silicate structures are sparse [7–10].

The structural unit of silicates is the SiO_4 tetrahedron. By sharing oxygens, these units can combine to form larger ionic complexes (polyanions), which exhibit various shapes and sizes. Depending on the chemical conditions, these complexes can condense into large polymeric species, and eventually into a three-dimensional network. The transport properties

0953-8984/94/469835+18$19.50

of silicate melts obviously depend on the degree of networking, and on the facility with which the structure can incorporate mobile ions. In binary metal oxide silicates, M_xO–SiO_2, structural components include $M^{(2/x)+}$ and O^{2-} ions and a distribution of polyanions, which can be perceived as the result of a dynamic equilibrium of condensation and splitting reactions between polyanions of different extents. The general form of these reactions is

$$Si_nO_{3n+1}^{2(n+1)-} + SiO_4^{4-} \overset{k_{1,n}}{\rightleftharpoons} Si_{n+1}O_{3n+4}^{2(n+2)-} + O^{2-} \tag{1}$$

where the reaction constants $k_{1,n}$ are defined as

$$k_{1,n} = \frac{[Si_{n+1}O_{3n+4}^{2(n+2)-}][O^{2-}]}{[Si_nO_{3n+1}^{2(n+1)-}][SiO_4^{4-}]}. \tag{2}$$

Here $[Si_nO_{3n+1}^{2(n+1)-}]$, $[Si_{n+1}O_{3n+4}^{2(n+2)-}]$ and $[O^{2-}]$ are anion fractions, and will henceforth be abbreviated as X_n, X_{n+1} and $X_{O^{2-}}$, respectively. By assuming that the $k_{1,n}$ are independent of composition, length and form of polyanions, Masson *et al* [1,2] derived a formalism that allows for the calculation of the polyanion distributions in silicate systems. A detailed review of the models for silicate melts has been given by Gaskell [3].

Recently the system CoO–SiO_2 has been systematically investigated by Kieffer and Borchardt [11,13] and by Young *et al* [14]. Kieffer and Borchardt [11,13] proposed a kinetic model that accounts for polycondensation reactions between network species and for diffusional transport. As opposed to the common thermodynamic approaches [1–6], this model allows one to consider non-equilibrium situations and to observe the evolution of the system as a function of time. The authors applied their model to evaluate polyanion distributions and effective cation tracer diffusion coefficients in the system CoO–SiO_2, as a function of composition. Subsequently, Young *et al* [14] measured the tracer diffusion coefficients of oxygen as a function of temperature and composition.

In the work presented here, the kinetic theory of Kieffer and Borchardt [13] has been enhanced to encompass oxygen tracer diffusion in silicate melts. While it is straightforward to account for the number of silicon atoms incorporated in a j-mer, the number of oxygen atoms carried by this aggregate depends on the extent of internal crosslinking. In the original formulation of the model, this information was implicitly contained in factors $w(j,m)$, which represent the probabilities for a j-mer to emanate from an m-mer, where $m > j$, through rupture of a single bond. An explicit expression for the $w(j,m)$ is impossible to give without extensive knowledge of structural geometries. In the present work we therefore simplified the original formulation in order to be able to incorporate an explicit oxygen balance. In the following we will briefly outline the derivation of the revised equations, and then show how the model can be applied to explain the experimentally observed behaviour of oxygen tracer diffusion in cobalt silicate melts. Furthermore, the polyanion distributions in this system, as calculated with the revised model, will be given. Finally, simulations of oxygen and silicon tracer diffusion in the systems CaO–SiO_2 and PbO–SiO_2 will be discussed.

2. Kinetic model of silicate melts

2.1. Structure of silicate melts

In their original derivation, Kieffer and Borchardt attempted to incorporate the complexity of network structure of silicate melts by means of a functionality parameter f_j and a related

factor $w(j, m)$, describing the probability that an m-mer decomposes to yield at least one j-mer. This combination of factors reflects the fraction of bridging oxygens that a polyanion of a given size can have. The authors chose the magnitudes for the functionality parameter as a function of the composition, by interpolating between known limiting values. They described the system by means of anion fractions N_j, where j is the number of silicon atoms incorporated into a polyanion containing j unit building blocks. It is defined as

$$N_j = n_j \Big/ \sum_{i=1}^{\infty} i n_i \tag{3}$$

where n_j is the number of polyanions with j silicon atoms.

They took the value of the equilibrium reaction constant $k_{1,n} = 2.6$ for $CoO–SiO_2$ at $T = 1450\,°C$ from Masson [2]. Furthermore, the magnitude of $k_{1,n}$ was assumed to be independent of the size of polyanion, and according to equation (1) can be related to the reaction rate constants k^+ for condensation and k^- for splitting, according to $k_{1,n} = k^+/k^-$. The overall equilibrium polyanion distributions can then be calculated by solving the system of coupled reaction rate equations. The numerical results for the polyanion distribution in cobalt silicate melts show a good qualitative agreement with those of Masson [2].

As a result of the condensation and splitting reactions, silicon tracer atoms are exchanged between polyanions of different sizes, and, depending on the size of the polyanion they are incorporated in, the silicon tracer atoms migrate with different velocities. When combining (de)polymerization reactions and Fick's transport equations, the development of tracer concentration profiles with time can be simulated for various chemical and thermal conditions. Here we will expand this formalism to include the balance of oxygen atoms. To this end we will introduce two minor modifications to the original formulation:

(i) With the adjustable $w(j, m)$ parameters Kieffer allowed, in principle, for various degrees of ramification and ring formation in the polyanions. In his calculations he chose the values for $w(j, m)$ arbitrarily within known limits. Unfortunately, the same value for $w(j, m)$ can be obtained for different polyanion geometries. Since the oxygen balance depends on the knowledge of the relative extent of ring formation versus open-ended branching, we needed a more definite approach here. Because of the relatively small effect that $w(j, m)$ has on the polyanion distributions, we simply incorporated it into the reaction rate coefficient k^-. For compatibility reasons we therefore replaced the factor $(j - 1)$, which represents the number of bonds within a j-mer that can break, with the factor $\mu(j)$. The magnitude of the latter factor can vary; for linear chains it will again be $(j - 1)/2$. Furthermore, since the reaction constant k is assumed to be independent of polyanion shape and size, any size dependence of the reaction rate constant will drop out in the end.

(ii) The oxygen will be accounted for as being part of aggregates of various sizes, including free oxygen O^{2-}. It is therefore advantageous to normalize the anion fractions by including the free oxygen, i.e.

$$X_j = n_j \Big/ \left(\sum_{i=1}^{\infty} n_i + n_{O^{2-}} \right) \tag{4}$$

where $n_{O^{2-}}$ is the number of free oxygen anions in the system and n_j is the number of polyanions of size j. Naturally these anion fractions are normalized to unity:

$$X_{O^{2-}} + \sum_{j=1}^{\infty} X_j = 1. \tag{5}$$

For the following derivation it is assumed that a series of reactions, all extensions of equation (1), contribute to the overall anion balance. The general form of these reactions can be written, after Masson, as

$$m + (j - m) \underset{k^-}{\overset{k^+}{\rightleftharpoons}} j + O^{2-}. \tag{6}$$

Within a balance of volume $dx\,dy\,dz$, small compared to the root-mean-squared displacement of the mobile species during the observation period, but large compared to the average polyanion chain length , the anion balance can be established by including condensation and splitting reactions, as well as diffusion fluxes for each individual species simultaneously. After Kieffer [12, 13] the balance for a j-mer in one dimension includes the following three processes:

1. *Diffusion* of j-mers

$$\frac{\partial X_j}{\partial t} = \frac{\partial}{\partial x}\left(D_j \frac{\partial X_j}{\partial x}\right) = D_j \frac{\partial^2 X_j}{\partial x^2} \tag{7}$$

with a diffusion coefficient D_j that is independent of the chemical composition.

2. *Creation* of a j-mer through

(i) condensation of an m-mer with a $(j - m)$-mer

$$\frac{\partial X_j}{\partial t} = k^+ \sum_{m=1}^{\lambda(j)} X_m X_{j-m} \tag{8}$$

(ii) splitting of an m-mer when reacting with a free oxygen

$$\frac{\partial X_j}{\partial t} = k^- \sum_{m=j+1}^{\infty} X_m X_{O^{2-}} \tag{9}$$

where $\lambda(j)$ is the integer part of fraction $j/2$ in order to avoid double counting.

3. *Annihilation* of a j-mer through

(i) condensation of a j-mer with any other m-mer to a $(j + m)$-mer

$$\frac{\partial X_j}{\partial t} = -k^+ X_j \sum_{m=1}^{\infty} X_m \tag{10}$$

(ii) splitting of a j-mer with free oxygen ions

$$\frac{\partial X_j}{\partial t} = -k^- X_{O^{2-}} \mu(j) X_j \tag{11}$$

where $\mu(j)$ is the set of possibilities for a j-mer to decompose into smaller fragments. If no rings form, there are $(j - 1)$ bonds in the polyanion, and $\mu(j)$ is equal to $(j - 1)/2$. The factor of $1/2$ is due to symmetry.

Summation of the above equations yields

$$\frac{\partial X_j}{\partial t} = D_j \frac{\partial^2 X_j}{\partial x^2} + k^+ \sum_{m=1}^{\lambda(j)} X_m X_{j-m} + k^- \sum_{m=j+1}^{\infty} X_m X_{O^{2-}} - k^+ X_j \sum_{m=1}^{\infty} X_m - k^- X_{O^{2-}} \mu(j) X_j. \tag{12}$$

Equation (12) describes the local ion balance of polymer ions of any size j; the entire system of polyanions is described by an infinite number of similar equations, one for every j-mer. In practice, one has to limit this number of equations, which is reasonable to do, as long as the anion fractions converge to 0 for $j \to \infty$, i.e. for sufficiently large modifier cation concentrations.

A special case is that of the equilibrium state. Then the X_j are independent of time and space, i.e.

$$\partial X_j / \partial x = 0 \qquad \text{and} \qquad \partial X_j / \partial t = 0.$$

Equation (12) then reduces to

$$k^+ \sum_{m=1}^{\lambda(j)} X_m X_{j-m} + k^- \sum_{m=j+1}^{\infty} X_m X_{O^{2-}} - k^+ X_j \sum_{m=1}^{\infty} X_m - k^- X_{O^{2-}} \mu(j) X_j = 0. \tag{13}$$

Using equation (5), which is rewritten as

$$\sum_{j=1}^{\infty} X_j = 1 - X_{O^{2-}}$$

we get

$$\sum_{j+1}^{\infty} X_m = 1 - X_{O^{2-}} - \sum_{m=1}^{j} X_m = 1 - X_{O^{2-}} - \sum_{m=1}^{j-1} X_m - X_j$$

and equation (13) becomes

$$k^+ \sum_{m=1}^{\lambda(j)} X_m X_{j-m} + k^- X_{O^{2-}} \left(1 - X_{O^{2-}} - \sum_{m=1}^{j-1} X_m - X_j\right) - k^+ X_j (1 - X_{O^{2-}}) - k^- X_{O^{2-}} \mu(j) X_j = 0.$$

Dividing the above equation by k^-, using $k = k^+/k^-$, and regrouping all X_j terms to the left-hand side, we get

$$X_j [X_{O^{2-}} + k(1 - X_{O^{2-}}) + \mu(j) X_{O^{2-}}] = k \sum_{m=1}^{\lambda(j)} X_m X_{j-m} + X_{O^{2-}} \left(1 - X_{O^{2-}} - \sum_{m=1}^{j-1} X_m\right).$$

One can solve this expression for X_j:

$$X_j = \left[k \sum_{m=1}^{\lambda(j)} X_m X_{j-m} + X_{O^{2-}} \left(1 - X_{O^{2-}} - \sum_{m=1}^{j-1} X_m\right)\right] [X_{O^{2-}} + k(1 - X_{O^{2-}}) + \mu(j) X_{O^{2-}}]^{-1}. \tag{14}$$

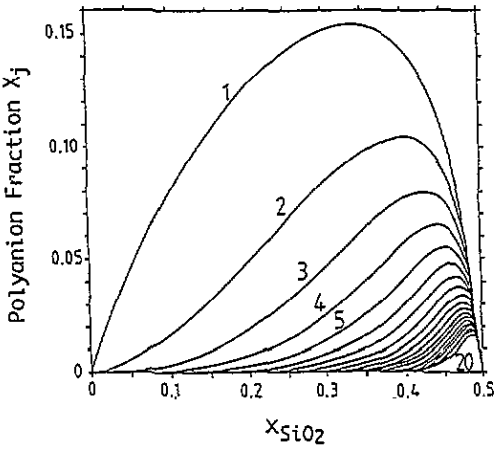

Figure 1. Polyanion distribution as a function of the silica concentration in CoO–SiO_2 melts, calculated by using the present model. The curves are for $j = 1$ to 20.

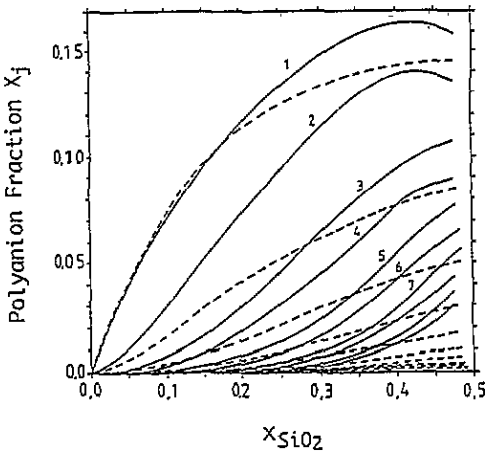

Figure 2. Polyanion distribution as a function of the silica concentration, calculated by using different models: (——) after Masson [2]; (- - - -) after Kieffer [13]. The curves are for $j = 1$ to 10.

For the monomer fraction, this equation simplifies to

$$X_1 = \frac{X_{O^{2-}}(1 - X_{O^{2-}})}{k(1 - X_{O^{2-}}) + X_{O^{2-}}}. \tag{15}$$

This expression is identical to that given by Masson for the monomer fraction [1,2]. In figure 1 the results from this work, including anion fraction up to $j = 20$, for system CoO–SiO_2 are shown. Again, the value of 2.6 was assumed for k. For comparison, we show in figure 2 the polyanion distributions calculated using the original formulation by Kieffer [11, 13], and those reported by Masson. The agreement is rather qualitative.

In equation (14) the fraction of a j-mer is expressed as a function of all the n-mers with $n < j$, and the fraction of free oxygen. The relation to the chemical composition of the system is obtained as follows. The number of silicon atoms is given by

$$c_{SiO_2} = \sum_{j=1}^{\infty} jn_j = F \sum_{j=1}^{\infty} jX_j \tag{16}$$

where n_j are the number of polyanions of size j, and

$$F = \sum_{j=1}^{\infty} n_j + n_{O^{2-}}$$

is the normalization factor from equation (4). The product $jn_j = jFX_j$ is equal to the number of silicon atoms in the j-mer, and will be referred to as c_j. Similarly, $c_{O^{2-}} \equiv n_{O^{2-}} = FX_{O^{2-}}$. On the other hand, let c_{O_j} be the number of oxygens per j-mer. The total oxygen balance then reads

$$c_{O^{2-}} + \sum_{j=1}^{\infty} c_{O_j} = c_{MO} + 2c_{SiO_2} = c_{O_{total}}. \tag{17}$$

At this point it is necessary to make assumptions concerning the cyclization within each polyanion. For the work reported here our choice was to consider rings composed of no less than six units. Hence,

$$c_{O_j} = \begin{cases} (3j+1)n_j = (3j+1)FX_j & \text{for } j < 6 \\ (3j+1)n_j(1-x) + x(2jn_j) = F[(3j+1)X_j - x(j+1)X_j] & \text{for } j \geqslant 6 \end{cases}$$

where x represents the fraction of non-linear polyanions. Note that if X_{SiO_2} approaches 1, then $c_{O_j} = 2jc_j$. Although the possibility of threefold rings has been postulated by Bockris *et al* [15], in this work we only assumed rings larger than six units for the system CoO–SiO_2, based on the results by Smith and Masson [2], who reported predominantly linear polyanions. Substitution in equation (22) yields

$$c_{O^{2-}} + \sum_{1}^{5}(3j+1)n_j + \sum_{6}^{\infty} n_j[(3j+1) - x(j+1)] = c_{O_{total}}$$

and after regrouping

$$c_{O^{2-}} + \sum_{1}^{\infty}(3j+1)n_j - x\sum_{6}^{\infty}(j+1)n_j = c_{O_{total}}. \tag{18}$$

Using equations (16) and (5) we can replace the first two terms on the left-hand side of equation (18) and get

$$x\left(\sum_{6}^{\infty} jn_j + \sum_{6}^{\infty} n_j\right) = 3n_{SiO_2} + F - c_{O_{total}} = n_{SiO_2} + F - n_{MO}. \tag{19}$$

Using the same assumptions concerning cyclization, we can furthermore express the numbers of singly bonded oxygens, O^-, and bridging oxygens, O^0, as

$$c_{O^-} = \sum_{1}^{5}(2j+2)n_j + \sum_{6}^{\infty}(2j+2)n_j(1-x) = \sum_{1}^{\infty}(2j+2)n_j - x\sum_{6}^{\infty}(2j+2)n_j \tag{20}$$

and

$$c_{O^0} = \sum_{1}^{5}(j-1)n_j + \sum_{6}^{\infty}[(j-1)n_j(1-x) + x(2jn_j)] = F\left(\sum_{1}^{\infty}(j-1)X_j + x\sum_{6}^{\infty}(j+1)X_j\right). \tag{21}$$

In both equations (20) and (21), we can eliminate the rightmost summation using equation (19), and we can express the concentrations of the oxygen species, O^0 and O^-, as functions of the chemical composition and the amount of free oxygen O^{2-}:

$$n_{O^-} = 2\left(\sum_{1}^{\infty}(j+1)n_j - n_{SiO_2} - F + n_{MO}\right) = 2(n_{SiO_2} - n_{O^{2-}} + F - n_{SiO_2} - F + n_{MO})$$

and it follows that

$$n_{O^-} = 2(n_{MO} - n_{O^{2-}}). \tag{22}$$

Similarly, we find

$$n_{O^0} = 2n_{SiO_2} + n_{O^{2-}} - n_{MO}. \tag{23}$$

Therefore the only input data that we need for our calculations are the concentration of free oxygen and the polycondensation equilibrium constant. Our calculations are based on the values reported by Masson for these two quantities [1, 2]. In figure 3 the relative amounts of O^{2-}, O^0 and O^- are shown for the system CoO–SiO_2. In summary, the principal differences between the current formulation of the kinetic model and Kieffer's original form are the assumption of experimental data for the O^{2-} concentration and the ability to compute anion fractions recursively, as described by equations (14) and (15).

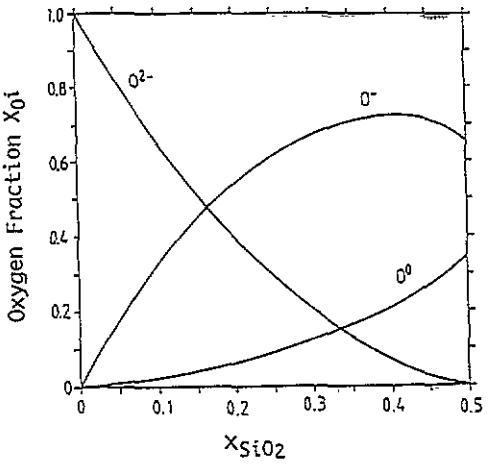

Figure 3. Oxygen species distribution in CoO–SiO_2 melts.

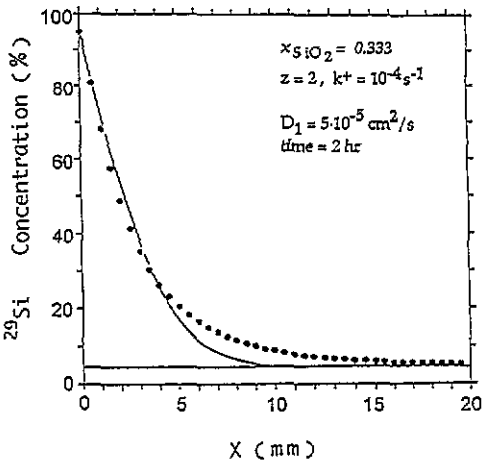

Figure 4. Simulated concentration profile for Si tracer diffusion (dots) in CoO–SiO_2 assuming constant surface concentration. The full curve represents the analytical solution for the same initial and boundary conditions, assuming a constant diffusion coefficient.

2.2. *Silicon and oxygen tracer diffusion in polyanion melts*

Assuming an equilibrium polyanion distribution, as obtained by the above procedure, we can substitute a fraction of the elements by a different isotope. Owing to the incorporation of Fick's second law in the balance equations, tracer concentration profiles for various initial and boundary conditions can be simulated. Substituting $c_j = jFX_j$ in equations (7)–(11), the time-dependent change of j-mer becomes

$$\frac{\partial c_j}{\partial t} = D_j\frac{\partial^2 c_j}{\partial x^2} + \frac{j}{F}k^+\sum_{m=1}^{\lambda(j)}\frac{c_m}{m}\frac{c_{j-m}}{j-m} + \frac{j}{F}k^-\sum_{m=j+1}^{\infty}\frac{c_m}{m}c_{O^{2-}} - \frac{k^+}{F}c_j\sum_{m=1}^{\infty}\frac{c_m}{m} - \frac{k^-}{F}\mu(j)c_{O^{2-}}c_j. \tag{24}$$

2.2.1. Tracer diffusion of silicon. Suppose that a silicon tracer isotope is introduced into the melt. We can assume that it is uniformly distributed over all j-mers, i.e. for $t = 0$ the fraction of tracer isotopes, x_j^T, is a constant for all j-mers. The balance of tracer elements is obtained my multiplying each concentration in equation (24) by the respective fraction of substituted isotopes. Abbreviating $c_j^* = c_j x_j^T$, we get

$$\frac{\partial c_j^*}{\partial t} = D_j\frac{\partial^2 c_j^*}{\partial x^2} + \frac{k^+}{F}\sum_{m=1}^{\lambda(j)}\left(c_m^*\frac{c_{j-m}}{j-m} + c_{j-m}^*\frac{c_m}{m}\right) + \frac{j}{F}k^-c_{O^{2-}}\sum_{m=j+1}^{\infty}\frac{c_m^*}{m} - \frac{k^+}{F}c_j^*\sum_{m=1}^{\infty}\frac{c_m}{m} - \frac{k^-}{F}\mu(j)c_{O^{2-}}c_j^*. \tag{25}$$

Furthermore, the total tracer concentration is $c^* = c_1^* + c_2^* + \cdots = \sum c_j^*$ and therefore

$$\frac{\partial c^*}{\partial t} = \sum_{j=1}^{\infty}\frac{\partial c_j^*}{\partial t}.$$

The numerical simulation of tracer diffusion in a polyanion melt is carried out using an explicit finite-difference method to represent equation (25) numerically. The ion fraction $X_{O^{2-}}$ is obtained from the activity of CoO [1,2]. If instead of $k = 2.6$, after Masson, we use $k = 2.39$ following Gaskell [3], the results for CoO–SiO_2 melt simulations yield no significant difference. The important detail that makes the outcome of these simulations non-trivial is the assumption that tracer elements migrate with different velocities, depending on the size of the polyanion they are incorporated in. The relative mobility of different polyanions can be described by a relation proposed by de Gennes [16], according to which the diffusion coefficients depend on the mass of the molecule as

$$D_j = D_1(M_j/M_1)^z. \tag{26}$$

A reasonable value for the diffusivity of the smallest polyanion is $D_1 = 5\times10^{-5}$ cm^2 s^{-1} [12, 13]. The simulation starts with initial conditions of either a constant surface concentration or a source of finite thickness. Equation (25) was solved for a finite number of j-mers, up to 20 for $X_{SiO_2} = 0.333$ and up to 35 for $X_{SiO_2} = 0.428$. The maximum j-value was chosen such as to guarantee a reasonable convergence in the anion fractions, i.e. vanishing fractions of the largest anions. The time increment for the integration was chosen to be 1 s.

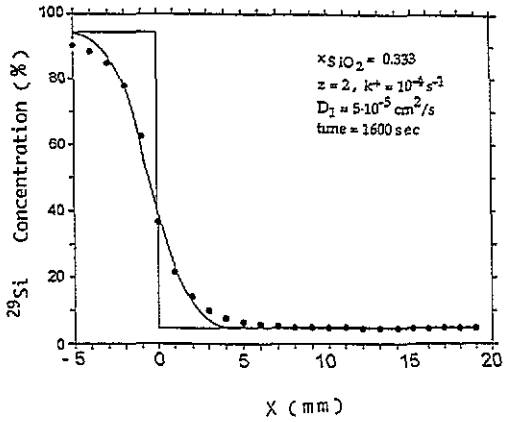

Figure 5. Calculated silicon tracer diffusion profile (dots) in CoO–SiO_2, assuming the same initial boundary conditions as in experiments by Kieffer [11], using $k = 2.6$, $z = 2$, $D_1 = 5 \times 10^{-5}$ cm^2 s^{-1}. The full curve represents the analytical solution for the same initial and boundary conditions, assuming a constant diffusion coefficient.

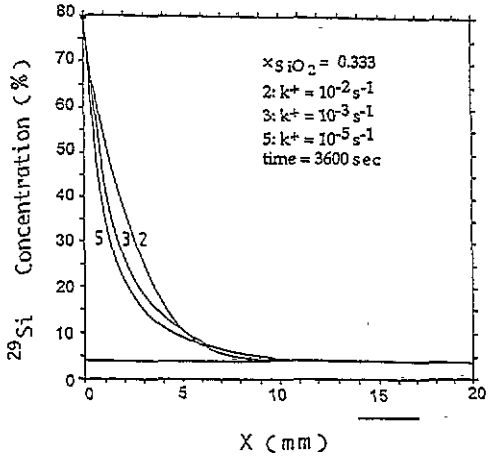

Figure 6. Simulation of Si diffusion with constant surface concentration, using $k = 2.6$, $t = 3600$ s, $z = 2$ and $D_1 = 5 \times 10^{-5}$ cm^2 s^{-1}.

In figure 4 the concentration profiles so obtained are shown for the case of a constant boundary concentration. The dots represent the simulation results, and the full curve is the best fit of these data with a standard error function complement solution, assuming a constant diffusion coefficient. Note the discrepancy between the two. Analogously, in figure 5 the results for a finite source and the corresponding fit with the appropriate analytical solution are shown. This initial condition corresponds to those of experiments carried out in this

laboratory [12]. The discrepancy between simulation results and analytical fits is strongly dependent on the form of the polyanion distribution, as we will show later when comparing these data to those from simulations of the systems $CaO–SiO_2$ and $PbO–SiO_2$ under the same initial and boundary conditions.

In figure 6 we show simulated silicon tracer diffusion profiles for situations characterized by different polycondensation rates, k^+. We recognize that, for a slower exchange of tracer isotopes between polyanions, the initial drop in the concentration profile is more rapid, but the tail of the concentration profile extends further into the specimen, which is due to the unimpeded migration of small anions. By impediment we mean condensation to a larger, slower-moving polyanion.

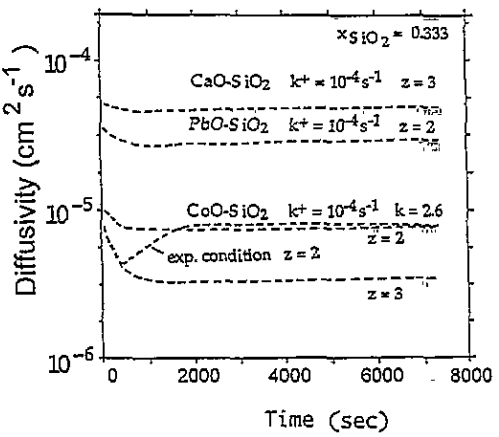

Figure 7. Effective silicon diffusion coefficients as a function of time, determined by a best fit of the analytical solution of Fick's second law for constant diffusion coefficients, to the simulation data.

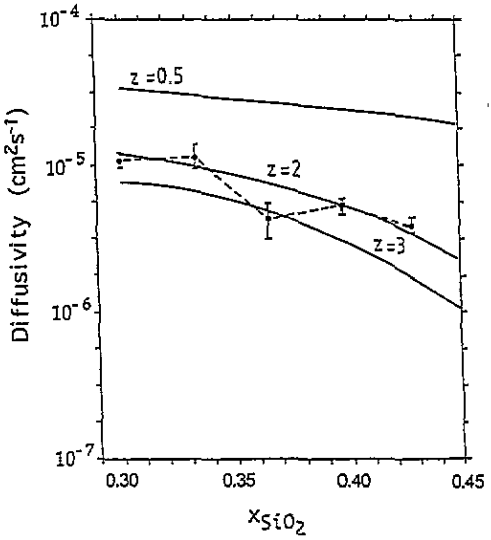

Figure 8. Effective tracer diffusion coefficient of silicon (——) compared to experimental data (— · —) by Kieffer, using $T = 1500\,°C$, $k = 2.6$, $k^+ = 10^{-4}\ s^{-1}$, $D_1 = 5 \times 10^{-5}\ cm^2\ s^{-1}$.

Effective diffusion coefficients, D_{eff}, have been determined by fits of analytical solutions to the simulated diffusion profiles. In general, D_{eff} is a function of the parameters k^+, z and D_1, as well as the diffusion time. In figure 7 the effective diffusion coefficients, determined from simulations, are shown as a function of the diffusion time, for various silicate systems. Below 2000 s a definite change in D_{eff} can be observed. The effect of time is even more significant in the case of SiO_2-rich melts. The same phenomenon has also been found by Kieffer [12, 13].

The values for the parameters k^+, z and D_1 can be estimated by comparing effective diffusivities to those obtained from experiment. In figure 8 the comparison between simulated and experimental results is shown for the case of silicon diffusion in $CoO–SiO_2$ systems [11]. The concentration dependences of the modelled and measured D_{eff} are in good qualitative agreement.

2.2.2. Tracer diffusion of oxygen. Although in principle similar to the description of silicon diffusion, oxygen diffusion requires one to account for one more level of complexity, which

arises from the distinct behaviour of free oxygen, O^{2-}, compared to singly or doubly bonded oxygen, O^- and O^0 respectively. The latter two species will be referred to as O_j, where j indicates the size of the polyanion they are incorporated in. Furthermore, depending on how the tracer source has been prepared, i.e. whether the oxygen tracer isotope has been brought in via the transition-metal oxide ($Co^{18}O$–SiO_2) or via the silicon dioxide (CoO–$Si^{18}O_2$), the initial conditions for the tracer distribution may be different [7, 17]. The fraction of tracer x_O^T would be different among free and networked oxygen atoms, if the condensation and splitting reactions were slow, and the degree of cyclization were large. The extreme cases of initial tracer distribution will be discussed below.

Of the two species O^- and O^0, only O^- can detach from a polyanion to form a free oxygen, within a single condensation reaction. However, if the oxygen tracer was brought in via the silica, one can assume that ^{18}O is distributed evenly over singly and doubly bonded oxygen atoms. We therefore do not differentiate between the two oxygen types, but rather distinguish oxygens according to the size of the anion they belong to. Hence, the diffusion rates of the different O_j species vary in the same way as those of the silicon species; in addition, O^{2-} exhibits a significantly higher mobility.

The balance of oxygen can be written:

$$\frac{\partial c_O}{\partial t} = \frac{\partial c_{O^{2-}}}{\partial t} + \sum_{j=1}^{\infty} \frac{\partial c_{O_j}}{\partial t} \tag{27}$$

where each partial differential on the right-hand side can be equated to a diffusional and a sum of reaction terms, as will be shown below. After introducing the factors f_j, where

$$f_j = \begin{cases} 3j+1 & j < 6 \\ 3j+1-x(j+1) & j \geqslant 6 \end{cases}$$

such that $c_{O_j} = f_j F X_j$, we can modify equations (8)–(11) to yield

$$\frac{\partial X_j}{\partial t} = k^+ \sum_{m=1}^{\lambda(j)} X_m X_{j-m} = k^+ \sum_{m=1}^{\lambda(j)} \frac{c_{O_m}}{f_m F} \frac{c_{O_{j-m}}}{f_{j-m} F} = \frac{k^+}{F^2} \sum_{m=1}^{\lambda(j)} \frac{c_{Om}}{f_m} \frac{c_{O_{j-m}}}{f_{j-m}} \tag{28}$$

$$\frac{\partial X_j}{\partial t} = k^- \sum_{m=j+1}^{\infty} X_m X_{O^{2-}} = \frac{k^-}{F^2} \sum_{m=j+1}^{\infty} \frac{c_m}{f_m} c_{O^{2-}} \tag{29}$$

$$\frac{\partial X_j}{\partial t} = -k^+ X_j \sum_{m=1}^{\infty} X_m = -\frac{k^+}{F^2} \frac{c_{O_j}}{f_j} \sum_{m=1}^{\infty} \frac{c_{O_m}}{f_m} \tag{30}$$

and

$$\frac{\partial X_j}{\partial t} = -k^- \mu(j) X_j X_{O^{2-}} = -\frac{k^-}{F^2} \mu(j) c_{O^{2-}} \frac{c_{O_j}}{f_j}. \tag{31}$$

Finally, after adding the diffusional term, the balance of oxygens associated with a j-mer reads

$$\frac{\partial c_{O_j}}{\partial t} = D_j \frac{\partial^2 c_{O_j}}{\partial x^2} + \frac{k^+ f_j}{F} \sum_{m=1}^{\lambda(j)} \frac{c_{O_m}}{f_m} \frac{c_{O_{j-m}}}{f_{j-m}} + \frac{k^- f_j}{F} \sum_{m=j+1}^{\infty} \frac{c_{O_m}}{f_m} c_{O^{2-}}$$
$$- \frac{k^+}{F} c_{Oj} \sum_{m=1}^{\infty} \frac{c_{O_m}}{f_m} - \frac{k^-}{F} \mu(j) c_{O^{2-}} c_{Oj}. \tag{32}$$

To describe the tracer diffusion of oxygen, we multiply each term in the above equation by the appropriate fraction of tracer isotopes. Note that the terms that diminish the oxygen balance within j-mers simply require multiplication by $x^{T}_{O_j}$, whereas the terms that enhance the balance do not. After a detailed account of what tracer fractions were present in the reactants, and how this translates into a fraction within the product, let $c^{*}_{O_j} = c_{O_j} \cdot x^{T}_{O_j}$, and we get

$$\frac{\partial c^{*}_{O_j}}{\partial t} = D_j \frac{\partial^2 c^{*}_{O_j}}{\partial x^2} + \frac{k^{+} f_j}{F} \sum_{m=1}^{\lambda(j)} \frac{1}{f_m + f_{j-m}} \left(c^{*}_{O_m} \frac{c_{O_{j-m}}}{f_{j-m}} + c^{*}_{O_{j-m}} \frac{c_{O_m}}{f_m} \right) + \frac{k^{-} f_j}{F} \sum_{m=j+1}^{\infty} \frac{1}{f_m + 1} \left(\frac{c_{O_m}}{f_m} c^{*}_{O^{2-}} + c^{*}_{O_m} c_{O^{2-}} \right) - \frac{k^{+}}{F} c^{*}_{O_j} \sum_{m=1}^{\infty} \frac{c_{O_m}}{f_m} - \frac{k^{-}}{F} \mu(j) c_{O^{2-}} c^{*}_{O_j}. \tag{33}$$

Again, this equation applies to the balance of oxygen contained in j-mers, where j can vary between 1 and ∞. It remains to establish the balance of free oxygen, which results from the following two contributions:

(i) The release of O^{2-} upon condensation of two polyanions,

$$\frac{\partial X_{O^{2-}}}{\partial t} = k^{+} \sum_{j=1}^{\infty} \left(\sum_{m=j}^{\infty} X_m X_j \right). \tag{34}$$

(ii) The consumption of O^{2-} upon a depolymerization reaction,

$$\frac{\partial X_{O^{2-}}}{\partial t} = -k^{-} \left(\sum_{j=2}^{\infty} X_{O^{2-}} \mu(j) X_j \right). \tag{35}$$

Summation of the two yields

$$\frac{\partial X_{O^{2-}}}{\partial t} = k^{+} \sum_{j=1}^{\infty} \left(\sum_{m=j}^{\infty} X_m X_j \right) - k^{-} X_{O^{2-}} \sum_{j=2}^{\infty} \mu(j) X_j. \tag{36}$$

Converting mole fractions into concentrations, using $c_{O^{2-}} = F X_{O^{2-}}$, and adding the appropriate diffusional term, the balance of free oxygen becomes

$$\frac{\partial c_{O^{2-}}}{\partial t} = D_{O^{2-}} \frac{\partial^2 c_{O^{2-}}}{\partial x^2} + \frac{k^{+}}{F} \sum_{j=1}^{\infty} \sum_{m=j}^{\infty} \frac{c_{O_m}}{f_m} \frac{c_{O_j}}{f_j} - \frac{k^{-}}{F} c_{O^{2-}} \sum_{j=2}^{\infty} \mu(j) \frac{c_{O_j}}{f_j}. \tag{37}$$

The fraction of tracer oxygens can then be introduced as before, using $c^{*}_{O^{2-}} = c_{O^{2-}} x^{T}_{O^{2-}}$ to yield

$$\frac{\partial c^{*}_{O^{2-}}}{\partial t} = D^{*}_{O^{2-}} \frac{\partial^2 c^{*}_{O^{2-}}}{\partial x^2} + \frac{k^{+}}{F} \sum_{j=1}^{\infty} \sum_{m=j}^{\infty} \left(\frac{c^{*}_{O_m}}{f_m + f_j} \frac{c_{O_j}}{f_j} + \frac{c^{*}_{O_j}}{f_m + f_j} \frac{c_{O_m}}{f_m} \right) - \frac{k^{-}}{F} c^{*}_{O^{2-}} \sum_{j=2}^{\infty} \mu(j) \frac{c_{O_j}}{f_j}. \tag{38}$$

The total oxygen tracer is obtained after substituting equations (38) and (33) into equation (27).

The numerical conditions for two different ways of introducing oxygen tracer, as indicated above, can be established as follows:

(i) *Oxygen tracers initially bonded to Co atoms.* It is generally assumed that the transition-metal oxides completely dissociate in the melt, so that all O* atoms at first will exist as free O^{2-} ions. At $t = 0$ all of the free oxygen will be enriched according to

$$c^*_{O^{2-}(x>0)} = x^T_{O(CoO)} c_{O^{2-}} \tag{39}$$

where $x^T_{O(CoO)}$ is the fraction of ^{18}O isotopes before mixing it with silica. Upon establishing thermodynamic equilibrium after mixing both oxides, part of the oxygens introduced through CoO has been used to break oxygen bridges, and will therefore be associated with polyanions,

$$c^*_{O_j(x>0)} = \frac{x^T_{O(CoO)}(c_{CoO} - c_{O^{2-}}) + f_{^{18}O} \sum c_{O_j}}{\sum c_{O_j}} c_{O_j} \tag{40}$$

where $f_{^{18}O}$ is the natural fraction of ^{18}O in oxygen.

(ii) *Oxygen tracers initially bonded to Si atoms.* If we assume that all O* atoms are first bonded to silicon atoms, the fractions of O^*_j are still less than the input value, because they are diluted by the formation of non-bridging oxygens, which require the incorporation of a free oxygen stemming from the CoO for every bond that is broken. Hence, at $t = 0$

$$c^*_{O_j(x>0)} = \frac{x^T_{O(SiO_2)} 2c_{SiO_2} + f_{^{18}O}(\sum c_{O_j} - 2c_{SiO_2})}{\sum c_{O_j}} c_{O_j} \tag{41}$$

and $c^*_{O^{2-}(x>0)}$ is equal to the natural fraction of ^{18}O,

$$c^*_{O^{2-}(x>0)} = f_{^{18}O} c_{O^{2-}}. \tag{42}$$

These two different initial conditions for the simulation of oxygen tracer diffusion were considered in order to compare the numerical results to those of experiments that we performed in our laboratory. In our experiments we used a capillary–reservoir technique, so that the boundary condition is a constant concentration at $x = 0$. The melt contained in the capillary was enriched. In figure 9 we show the simulated diffusion profile for these experimental boundary and initial conditions. The simulation, as for the experiment, was limited to a relatively short diffusion time, limited by the high diffusivity of O^{2-}. (With $L > 2(D_{O^{2-}}t)^{1/2}$, $t_{max} = 3600$ s for a $Co^{18}O$ tracer source.) The parameters for the simulation have been estimated, if not already known from the silicon tracer diffusion, by comparison with experimental data. From figure 9 it is again clear that the oxygen diffusion profiles cannot be fitted with the appropriate analytical solution.

3. Results and discussion

The accuracy of our computer simulations was verified by means of a situation for which the analytical solution is known. In the case of silicon diffusion, we determined a relative deviation from the exact result of 10^{-5} per iteration, where the time step was 1 s. For a typical simulation run, the relative error therefore amounts to about 1–3%. This inaccuracy is predominantly caused by the need to assume a finite value for the maximum length of a polyanion, j_{max}, instead of infinity. For the simulation of oxygen diffusion, the error

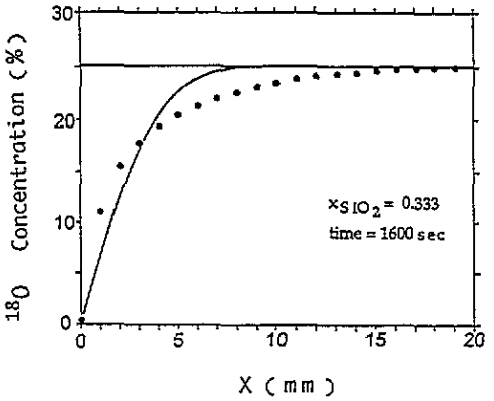

Figure 9. Simulated oxygen tracer diffusion profile for the system CoO–SiO_2 (dots). The full curve represents the analytical solution for the same initial and boundary conditions, assuming a constant diffusion coefficient. The simulation parameters are $k = 2.6$, $z = 2$, $k^{+} = 10^{-4}$ s^{-1}, $D_1 = 5 \times 10^{-5}$ cm^2 s^{-1}, $D_{O^{2-}} = 2 \times 10^{-4}$ cm^2 s^{-1}.

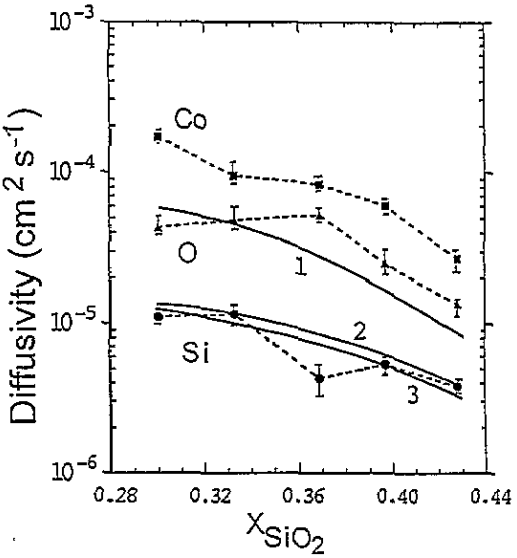

Figure 10. Effective tracer diffusion coefficients of Si and O in CoO–SiO_2 as a function of X_{SiO_2}, from both experiment [9, 10]: (■) ^{57}Co; (▲)^{18}O; (●) ^{29}Si, and simulations: 1, Co[18]; 2, $Si^{18}O_2$; 3, $^{29}SiO_2$.

accumulated at a rate of 2.5×10^{-5} per time step. For this reason the simulations were usually kept to about 1000 steps.

In figure 10 the results for the effective tracer diffusion coefficients of Si and O in the system CoO–SiO_2 are shown as a function of the melt composition. The concentration dependences in these coefficients are solely due to the shift in the polyanion distributions, and, with that, the shift in the average drift velocity of network species. For comparison, the numerical results are shown together with experimental data for the same system [11, 14]. This comparison demonstrates that our kinetic model provides a valid approach towards the interpretation of tracer diffusion of oxygen and silicon in CoO–SiO_2 melts, yielding good qualitative and quantitative agreement with the experiment. In figure 10, the curves labelled 1 to 3 represent the simulation results under the assumption of all tracer oxygen initially bonded to Co, tracer oxygen equally distributed among all species, and all tracer oxygen initially bonded to silicon, respectively. The effective oxygen diffusion is slowest when the tracer is brought in through the silicon only, and fastest when brought in through cobalt only. This behaviour was also observed in experiments. The same phenomenon has also been reported for the system CaO–SiO_2 [8]. Nevertheless, it seems to be extremely pronounced in the case of cobalt silicate melts. We therefore applied our model to the simulation of two other, well characterized systems, CaO–SiO_2 [17–19] and PbO–SiO_2 [9, 10] melts.

The polyanion distribution for lead and calcium silicates were calculated using equation (15). We have taken the values for the condensation equilibrium constants k from Masson [1]; they are $k = 0.0016$ for CaO–SiO_2 and $k = 0.196$ for PbO–SiO_2. For the activities of polyanions we used the values reported by Masson for branched polyanions. In figures 11 and 12 we present the polyanion distributions for CaO–SiO_2 and PbO–SiO_2

melts, according to our calculations. For comparison, we included Masson's results as broken curves. Our results are in excellent quantitative agreement with those of Masson. For mole fractions $X_{SiO_2} > 0.45$ this kinetic model yields even better convergence than the thermodynamic models. Until now anion fractions have only been reported up to $j = 10$, because of the poor convergence of some models. The sums over all anion fractions shown in figures 11 and 12, $\sum X_j$ towards the SiO_2-rich side are very close to 1 (for $X_{SiO_2} = 0.5$, $j = 20$ the error of $\sum X_j$ is smaller than 0.001%), but according to other models these sums are typically much greater than 1. For PbO–SiO_2 the calculated polyanion fraction is 2.3×10^{-6} for $j = 15$, whereas for CaO–SiO_2 it is 3.8×10^{-8} at $j = 12$. The fractions of larger polyanions can therefore be neglected. Knowing the polyanion distribution we have then calculated the distributions of O^0, O^- and O^{2-} for these systems. The results shown in figures 13 and 14 are in good agreement with earlier work by Pretnar [4].

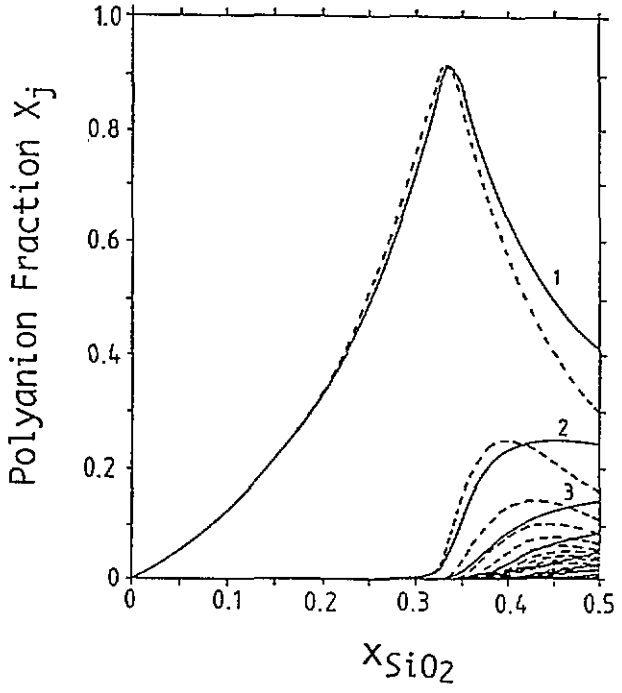

Figure 11. Polyanion distributions for CaO–SiO_2 melts with $k = 0.0016$, assuming the activities of branched polyanions reported by Masson [1]: (----) Masson; (——) this work. The curves are for $j = 1$ to 10.

The simulated profiles of silicon diffusion yield much better agreement with the analytical solution of Fick's law in the cases of CaO–SiO_2 and PbO–SiO_2 melts. The agreement with values reported in the literature is also very good. For polyanion diffusion we have used the same values for the parameters z and D_1 as we had estimated for CoO–SiO_2 melts. Figure 15 shows a fit of the analytical solution of Fick's law, with constant diffusion coefficient, to the simulated profile of silicon diffusing in PbO–SiO_2. Likewise for the system CaO–SiO_2, the effective diffusion coefficient providing the best fit of the analytical solution is virtually identical to the value obtained by experiment [9, 10, 17–19]. This behaviour is quite different to that observed for the system CoO–SiO_2, where we

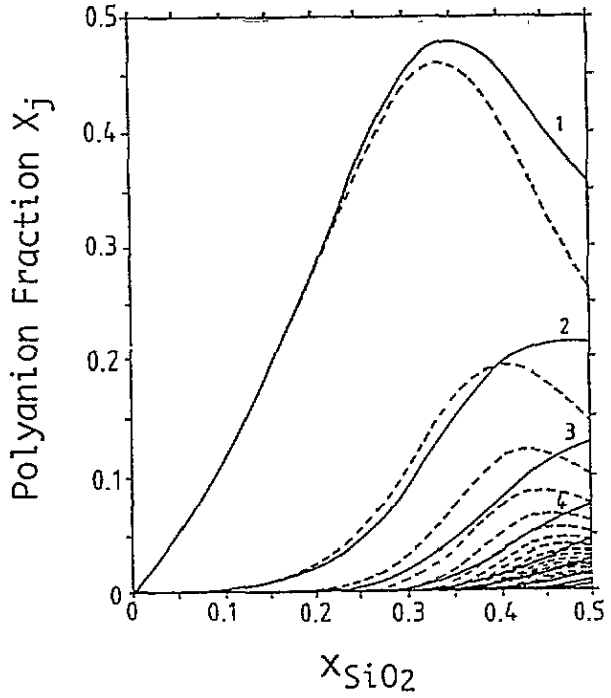

Figure 12. Polyanion distributions for $PbO–SiO_2$ melts with $k = 0.196$: (----) Masson; (——) this work. The curves are for $j = 1$ to 15.

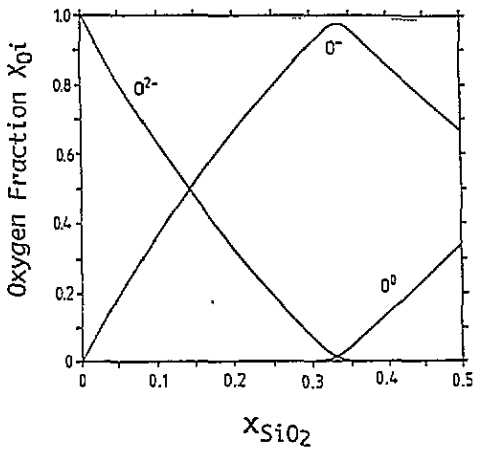

Figure 13. Distribution of O^0, O^- and O^{2-} for the system $CaO–SiO_2$ with $j = 20$, $k = 0.0016$.

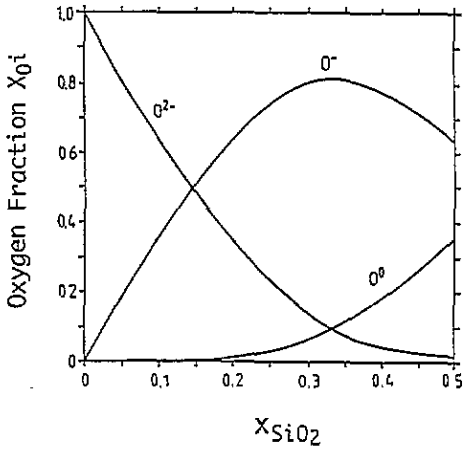

Figure 14. Distribution of O^0, O^- and O^{2-} for the system $PbO–SiO_2$ with $j = 20$, $k = 0.196$.

cannot get a good fit of the analytical solution to either simulated or experimental results for silicon and oxygen diffusion [11, 14].

In the present form our kinetic model does not include the migration of metal cations in an explicit way. In real life any concentration fluctuations of metal cations may have

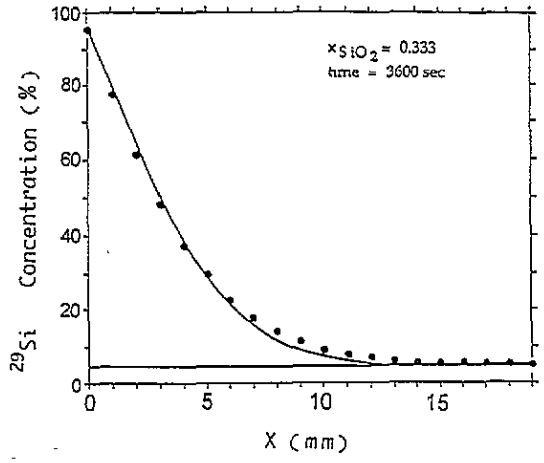

Figure 15. Simulation of a silicon tracer diffusion profile (dots) in PbO–SiO_2 and best fit with the corresponding analytical solution of Fick's second law, assuming a constant diffusion coefficient $D = (2.85 \pm 0.15) \times 10^{-5}$ cm^2 s^{-1}. The simulation parameters are $k = 0.196$, $z = 2$, $k^+ = 10^{-4}$ s^{-1}, $D_1 = 5 \times 10^{-5}$ cm^2 s^{-1}.

profound effects. For example, properties such as diffusion, viscosity and the melting point of silicates are strongly influenced by the nature and the concentration of metal cations. However, in our model the influence of the metal cations has been implicitly taken into consideration through the reaction equilibrium constant K and the value of D_1. Therefore, explicit consideration of the metal cation will most likely not affect the principal insights into the mechanisms of polyanion diffusion that were obtained by our kinetic model. Extending the model, in order to understand the role of metal cations, we need more detailed information concerning their interaction with the surrounding network, the type of information that may be gained by molecular dynamics simulations. Also, experimental work needs to be carried further in order to uncover the spectrum of structural environments present in these melts.

4. Conclusion

We have expanded the kinetic model of Kieffer and Borchardt to encompass oxygen tracer diffusion in silicate melts. Based on minor changes in the model assumptions, it was possible to derive a simple recursive formula for the calculation of polyanion distributions in silicate melts. The monomer (SiO_4^{4-} tetrahedron) concentration as a function of silica concentration calculated by this formula is identical to that resulting from the thermodynamic treatment by Masson. Based on the molar balances of the species present in the system, the diffusion equations of silicon and oxygen have been derived.

The effective tracer diffusion coefficients of oxygen and silicon have been determined by means of a best fit of simulated concentration profiles with the appropriate analytical solution for the same boundary and initial conditions, while assuming a constant diffusion coefficient. The same procedure has been applied to experimental data obtained in our laboratory. Based on the comparison between numerical and experimental results, the concentration dependence of the effective diffusion coefficients can be explained as due to

a distribution of effective drift velocities of the diffusing species, which results from their temporary incorporation into polyanions of various sizes.

A computer simulation of tracer diffusion of silicon and oxygen in the systems CoO–SiO_2, PbO–SiO_2 and CaO–SiO_2 revealed that the diffusion processes in CoO–SiO_2 are strongly influenced by the exchange of tracer species between polyanions of different sizes, whereas the diffusion in the other two systems, whose networks are far more disintegrated, can be described by a single diffusion coefficient with sufficient accuracy. The effective diffusion coefficients obtained by simulation are in good agreement with experimental results reported in the literature.

Acknowledgments

This work was supported by Deutsche Forschungsgemeinschaft. T F Young was awarded a scholarship of the Technische Universität Clausthal.

References

[1] Masson C R 1965 *Proc. R. Soc.* A **287** 201; 1968 *J. Am. Ceram. Soc.* **51** 134
Whiteway S G, Smith I B and Masson C R 1970 *Can. J. Chem.* **48** 33, 1432
Masson C R, Smith I B and Whiteway S G 1970 *Can. J. Chem.* **48** 201
[2] Masson C R, Smith I B and Whiteway S G 1970 *Can. J. Chem.* **48** 1456
Smith I B and Masson C R 1971 *Can. J. Chem.* 49 683
[3] Gaskell D R 1981 *Can. Met. Q.* 20 3
[4] Pretnar B 1968 *Ber. Bunsenges.* 72 773
[5] Lin P L and Pelton A D 1979 *Metall. Trans.* B **10** 667
[6] Kapoor M L, Mehrotra G M and Frohberg M G 1974 *Arch. Eisenhüttenwes.* 45 213, 663
[7] Saito T, Shiraishi Y, Nishiyama N, Sorimachi K and Sawada Y 1973 *Fourth Japan–USSR Joint Symp. on Physical Chemistry of Metallurgical Processes* Iron and Steel Institute of Japan, p 53
[8] Shiraishi Y, Nagahama H and Ohta H 1983 *Can. Met. Q.* 22 37
[9] Langanke B and Schmalzried H 1979 *Ber. Bunsenges. Phys. Chem.* **83** 59
[10] Schmalzried H, Takada Y and Langanke B 1981 *Z. Phys. Chem.* **128** 205
[11] Kieffer J, Borchardt G, Scherrer S and Weber S 1986 *Mater. Sci. Forum* 7 243
[12] Kieffer J and Borchardt G 1987 *Chem. Geol.* 62 93
[13] Kieffer J and Borchardt G 1989 *Glastech. Ber.* 62 337
[14] Young T F, Kieffer J and Borchardt G 1995 *J. Phys.: Condens. Matter* **6** 9825–34
[15] Bockris J O'M and Lowe D C 1954 *Proc. R. Soc.* A **226** 423
Bockris J O'M, Mackenzie J D and Kitchener J A 1955 *Trans. Faraday Soc.* **51** 1734
Bockris J O'M, Tomlinson J W and White J L 1956 *Trans. Faraday Soc.* **52** 299
[16] de Gennes P G 1971 *J. Chem. Phys.* 55 572
[17] Keller H, Schwerdtfeger K and Hennesen K 1979 *Metall. Trans.* B **10** 67
[18] Keller H and Schwerdtfeger K 1979 *Metall. Trans.* B **10** 551
[19] Keller H, Schwerdtfeger K, Petri H, Hölze R and Hennesen K 1982 *Metall. Trans.* B **13** 237